Supporting Information for:

Guest-induced symmetry lowering of an ionic clathrate material for carbon capture

Sanehiro Muromachi[a*], Konstantin A. Udachin[b], Kyuchul Shin[c], SamanAlavi[b,d], Igor L. Moudrakovski[d], Ryo Ohmura[e], and John A. Ripmeester[b]

[a] *Methane Hydrate Research Centre, National Institute of Advanced Industrial Science and Technology (AIST), 16-1 Onogawa, Tsukuba, 305-8569, Japan.*

[b] *National Research Council of Canada, 100 Sussex Drive, Ottawa, ON, K1A 0R6, Canada.*

[c] *Division of Ocean, Systems Engineering, Korea Advanced Institute of Science and Technology, Daejeon, 305-701, Republic of Korea.*

[d] *Department of Chemistry, University of Ottawa, Ottawa, ON K1N 6N5, Canada.*

[e] *Department of Mechanical Engineering, Keio University, Yokohama 223-8522, Japan.*

* Author to whom correspondence should be addressed. (S. M.)

Present address: AIST

E-mail: s-muromachi@aist.go.jp

Tell: +81-29-861-4287

Fax: +81-29-861-8706

Experimental and computational details

1. Single Crystal X-ray Diffraction Measurement

Single crystals of TBAB + CO_2 hydrates were formed in a high pressure glass cell with an inner volume of ~100 cm^3 and fitted with stainless-steel flanges at the ends so that the cell interior was observable. A ~30 mm diameter glass-vial with 5–10 cm^3 of aqueous TBAB solution was placed inside the pressure cell. The aqueous solutions of TBAB were prepared from a TBAB salt of 99% certified purity (Aldrich Chemical Company Inc.) and pure water (EMD Chemicals Inc., WX0004). The uncertainty in the mole fractions of TBAB in the aqueous solutions was ±0.0002, and that of the pressure was ±0.1 MPa. After degasification of the TBAB solution by a vacuum pump, charge and discharge procedures were repeated five times with 1 MPa of a CO_2 gas in order to eliminate the residual air. The pressure cell was charged with CO_2 gas up to the target pressure, and immersed in a temperature-controlled bath (Poly Science, VWR 1157). In order to avoid forming the TBAB hydrate without gas, we carefully controlled the bath temperature throughout the experiments to remain above the melting point of the pure TBAB ionic clathrate hydrate.[1-2] The temperature of the bath was first set to be ~1 K higher level than the equilibrium temperature for the TBAB + CO_2 hydrate to dissolve the CO_2 gas in the TBAB solution without forming pure TBAB hydrate. After dissolving the gas, the temperature was decreased to this target temperature. The purity of the CO_2 gas used was 99.99% on a volume basis which was provided by Praxair Inc. We used a mercury thermometer (Brooklyn Thermo Co., 76 mm) with an uncertainty of ±0.2 K for the temperature measurement. The *P*-*T*-*x* conditions for the formation of TBAB + CO_2 hydrates are available from the literature.[3,4–5] The single crystals were grown under the conditions that gave 1–3 K subcooling as is suitable for growing mm-sized crystals,[5,6] which were P = 1.08 MPa, T = 282.65 K, x_{TBAB} = 0.0064. After the completion of crystal formation (taking ~1 week), the high-pressure cell was chilled and the crystals were taken out at liquid nitrogen temperature. A suitably-sized single crystal was chosen by examination under a microscope with the crystals kept under a nitrogen atmosphere at ~230 K. The sample was handled and transferred to an X-ray diffractometer below this temperature and preserved at liquid-nitrogen temperature. The single crystal was mounted on an X-ray

diffractometer (Bruker Kappa APEX CCD), with data collection at 100 K. The models of the crystal structure were refined with SHELXTL software package.[7–8] CCDC 963037 contains the supplementary CIF crystallographic data for the presently found crystal structure. These data can be obtained free of charge from The Cambridge Crystallographic Data Centre via www.ccdc.cam.ac.uk/data_request/cif.

The refinement result for the TBAB + CO_2 ionic clathrate hydrate formed under the pressure P = 1.08 MPa, temperature T = 282.65 K and aqueous TBAB mole fractions x = 0.0064 is summarized in Table S1. A portion of the unit cell of the TBAB + CO_2 ionic clathrate hydrate is shown in Figure S1. The spatial relations between the D_A and D_B cages with the tert-butylammonium and bromide ions can be seen in this figure.

An interesting point in Table S2 is that the maximum CO_2 cage occupancy was obtained from the sample formed in the most dilute aqueous-TBAB solution with x = 0.0064. The cage occupancy (θ) was even higher than that of the sample formed at the higher pressure but in the nearly stoichiometric composition of the TBAB·38H_2O, i.e., with x = 0.0256. The reason for this can be the optimizing of the CO_2/TBAB ratio in the solution which can be the driver for CO_2 incorporation in the ionic clathrate hydrate phase.

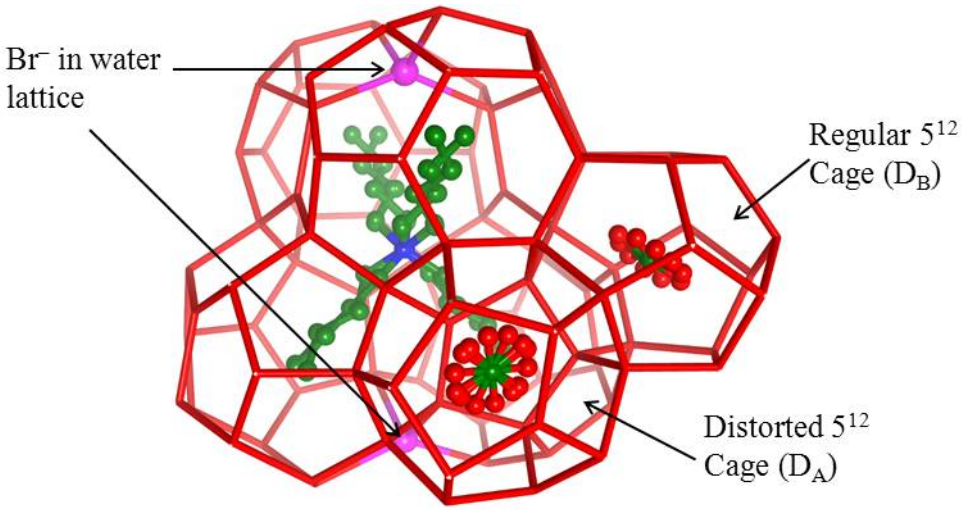

Figure S1. A section of the *Imma* unit cell of the TBAB + CO_2 ionic clathrate hydrate. The proximity of the Br^- ion in the water lattice to the distorted D_A cages can be seen in this figure.

Table S1. Crystal data and structure refinement results for the TBAB + CO_2 hydrate formed in the conditions (x = 0.0064, P = 1.08 MPa, T = 282.65 K).

Empirical formula	$C_{17.85}H_{111}BrNO_{41.69}$
Formula weight, g·mol^{-1}	1087.28
Temperature, K	100.0 (1)
Wavelength, Å	0.71070
Crystal system, space group	Orthorhombic, *Imma*
Unit cell dimensions, Å	a = 21.0197(7), b = 25.2728(8), c = 12.0096(4)
Volume, Å^3	6379.8(4)
Z, calculated density, g·cm^{-3}	4, 1.132
Absorption coefficient, μ	0.730
F(000)	2375
Crystal size, mm	0.6 × 0.4 × 0.2
θ range for data collection	2.52, 36.38
Index ranges	–35< h < 35 –35< k < 42 –20< l <19
Reflections collected/unique	87521/ 8002
Completeness to 2θ	0.98
Refinement method	F^2 against all reflections
Data/restraints/parameters	453/ 47/ 453
Goodness-of-fit on F^2	1.048
Final R indices [I > 2Σ(I)]	0.0266
R indices (all data)	0.0412
Largest diff. peak and hole	–0.48, 0.94

Table S2. The results of the SCXRD measurements for the orthorhombic TBAB·38H_2O·nCO_2 crystals formed under four different conditions.

x	P / MPa	T / K	n	θ_{DA}	θ_{DB}	$\theta_{average}$[a]
0.0256	1.13	286.05	1.36	0.761	0.301	0.454
0.0064	1.08	282.65	1.85	0.867	0.490	0.616
0.0357	1.16	286.25	1.52	0.797	0.359	0.505
0.0254	1.77	287.25	1.79	0.868	0.462	0.597

[a] The average occupancy of D cages in the framework of TBAB·38H_2O·D_A·2D_B.

2. NMR and Powder X-ray Diffraction Measurements

Samples suitable for solid-state NMR and powder X-ray diffraction (PXRD) measurements were prepared by taking a 1:38 TBAB solution in water, quenching the solution drop-wise in liquid nitrogen, then grinding the solid to a fine powder. The powdered solid was placed in a Pyrex tube fitted with a ground glass joint for connecting to a vacuum line. The sample was degassed, then ^{13}C enriched CO_2 (99.3% enrichment, Isotec) was condensed into the tube at 77 K and the tube was flame sealed. Samples were conditioned for a number of days at ~269 K. The ^{13}C solid state NMR measurements were obtained on Bruker Avance-III 400 MHz (magnetic field of 9.4 T) and Bruker Avance 200 MHz (magnetic field of 4.7 T) spectrometers. The measurements utilizing Magic Angle Spinning (MAS) were performed on a Bruker BL7 double resonance probe at the spinning rate of 3 kHz. The samples of hydrates prepared by the method outlined above were loaded into 7 mm OD ZrO_2 spinners in liquid nitrogen and then cold loaded into a probe pre-cooled to 173 K. Stationary spectra were obtained on a Bruker double resonance wide-line probe for solids with the samples stored in 5 mm sealed glass tubes also loaded with hydrate in liquid nitrogen. ^{13}C Cross-Polarization (CP) spectra were obtained using ramped contact pulses.[9] Both Bloch decay (single pulse) and the CP experiments were accompanied by high-power proton decoupling using the SPINAL64 decoupling scheme.[10-11] The temperature during the experiments was controlled using a Bruker BVT3000 temperature controller. Integration of the signals and powder pattern simulation were performed with the use of the DMFit simulation package.[12] The PXRD patterns of 1 : 38 TBAB and H_2O samples with and without CO_2 were recorded on a Bruker AXS model D8 Advance diffractometer using Cu K_α radiation (λ_1 = 1.5406 Å, λ_2 = 1.5444 Å, I_2/I_1 = 0.5). The finely powdered samples were quickly transferred to the pre-cooled X-ray stage and the diffraction patterns were measured at 173 K. The data were recorded in the step mode with a fixed time of 2 s and a step size of 0.010483° for 2θ = 6–50°. The patterns obtained were refined by Le Bail fitting using the profile matching method within FULLPROF.[13]

The integration of the CO_2 signals requires taking into account all of the spinning sidebands. The results of the integrations for the two samples studied are summarized in Table S3. A tentative

assignment of the CO_2 signals in the MAS spectra can be made based on the relative number of the cages in the structure.

Figure S2 shows stationary ^{13}C CP NMR spectra of the hydrate at temperatures ranging from 173 K to 233 K. A visible singularity in the spectrum at ~230 ppm indicates the presence of at least two superimposed powder patterns related to the different types of CO_2 molecules in the hydrate cages. The overall lineshape of the CO_2 signal in the spectrum is indicative of the chemical shift anisotropy. The overall width of the pattern is less than that expected for a rigid lattice and the roughly triangular shape is characteristic of a distribution in anisotropy values which arise from CO_2 molecules with dynamic properties that reflect the various cage environments that result when water molecules freeze into disordered positions.[14,15] Model calculations have illustrated likely motions of the long axis of the CO_2 molecules which are best described as limited amplitude librations.[14–16] The high frequency singularity in the spectrum is better visible in a higher field spectrum (Figure S2). The appearance of the singularity is characteristic of axial chemical shift anisotropy, with the singularity corresponding to the perpendicular component of the CSA tensor. Assuming an isotropic shift of 125 ppm, the powder pattern of this component can be isolated from the total spectrum as shown in Figure S3. However, this just serves to illustrate that there are two overlapping powder patterns. Since both will have characteristic and distinct distributions of the chemical shift anisotropy there are too many variables to extract meaningful quantitative fits to the total spectrum. The relative intensity of the signals suggests linking of the broader powder pattern and the MAS signal at the isotropic shift of 125.4 ppm. At higher temperature (Fig S2, 223 K), the lineshape starts to change. This has been associated with the onset of water reorientation, which gives the cages their true time averaged symmetry. For the oblate spheroidal cages (sI CO_2 hydrate large cage, CO_2 in the small cage in sII) the NMR powder pattern changes to that of an axially symmetric chemical shift characteristic of axial rotation in the cages. In general, the line shape reflects the symmetry of the cage, as isotropic, axial and non-axial lineshapes all have been observed.[17] From the spectrum at 223 K, it looks like water motions are becoming fast enough to start giving the cages their time-average symmetry.

The PXRD analysis explains the structural preference of TBAB hydrate depending on the presence of CO_2. The diffraction pattern obtained from 1 TBAB : 38 H_2O mixture without CO_2 (Figure S4a) shows mixed phases of tetragonal *P4/m* (a = 23.520(1) Å; c = 12.542(1) Å) and orthorhombic *Pmma* (a = 20.909(1) Å; b = 12.681(1) Å; c = 12.219(1) Å) with a small fraction of another tetragonal phase indexed to $P4_2/m$ (a = 23.711(1) Å; c = 12.318(1) Å). On the other hand, the pattern of TBAB hydrate with CO_2 (Figure S4b) shows mainly orthorhombic *Imma* structure (a = 21.190(1) Å; b = 25.405(1) Å; c = 12.049(1) Å) with a small fraction of the tetragonal $P4_2/m$ phase (a = 23.648(1) Å; c = 12.278(1) Å).

As mentioned above, the presence of CO_2 vapor might lead to the appearance of more orthorhombic phase, which possesses more 5^{12} cages for CO_2 inclusion, and thus the two main signals for CO_2 (natural abundance) appearing at 124.85 and 125.06 ppm of the ^{13}C NMR spectrum shown in Figure S5 should originate from the orthorhombic phase and the additional small peak at 125.30 ppm from a small fraction of the tetragonal $P4_2/m$ phase, respectively.

The lattice parameters obtained from the Le Bail fitting of the PXRD patterns all agree with the results of our single-crystal XRD refinement and the previously reported values in the literature.[18–23] Here, it is worthwhile to note that the structureless Le Bail fitting method cannot distinguish the *Imma* phase from *Pmma*, which is the previously reported space group of the TBAB hydrate crystal in the absence of gaseous guest[21], in the PXRD pattern of TBAB + CO_2 hydrate. Figure S6 shows the Le Bail fitting of the same pattern, but with orthorhombic *Pmma* indexing instead of *Imma*. We obtained the lattice parameters of a = 21.186(1) Å, b = 12.695(1) Å, and c = 12.035(1) Å with a reasonable goodness of fit value (χ^2 = 2.51) and quite similar a and c values with half a b-axis as compared to the *Imma* space group. This means that the symmetry lowering of the clathrate hydrate crystal is difficult to distinguish by powder diffraction pattern measurements. The guest-induced structural transformation accompanied by symmetry lowering described in this work is reminiscent of the temperature-induced symmetry lowering transition of hexagonal structure-H hydrate from *P6/mmm* to *P-3* at 167 K.[24] In this previous study, the simulated PXRD pattern of the *P6/mmm* structure was almost exactly the same as that for *P-3*, similar to the experimental results of our present work.

Table S3. Integrated intensities in ^{13}C MAS spectra (integration with summing of sideband intensities, 9.4 T data).

Carbon atom	Position, ppm	I_{total}%	Relative *I*, % normalized to CO_2
Sample: $^{13}CO_2$·TBAB·38H_2O; 2975 Hz CPMAS; $t_{cont.}$ = 5 ms			
TBAB-1	59.13	3.73	
TBAB-2'	25.42	2.03	
TBAB-2"	24.66	1.69	
TBAB-3'	21.05	1.59	
TBAB-3"	20.71	2.50	
TBAB-4	14.75	4.08	
CO_2-1	124.87	25.23	29.91
CO_2-2	125.13	46.71	55.36
CO_2-3	125.40	12.43	14.73
Sample: N.A. CO_2·TBAB·38H_2O; 3083 Hz CPMAS; $t_{cont.}$ = 5 ms			
TBAB-1	59.13	23.92	
TBAB-2'	25.45	11.72	
TBAB-2"	24.68	9.99	
TBAB-3'	21.09	10.28	
TBAB-3"	20.74	13.68	
TBAB-4	14.7	24.6	
CO_2-1	124.85	2.79	48.11
CO_2-2	125.06	2.71	46.72
CO_2-3	125.3	0.3	5.17

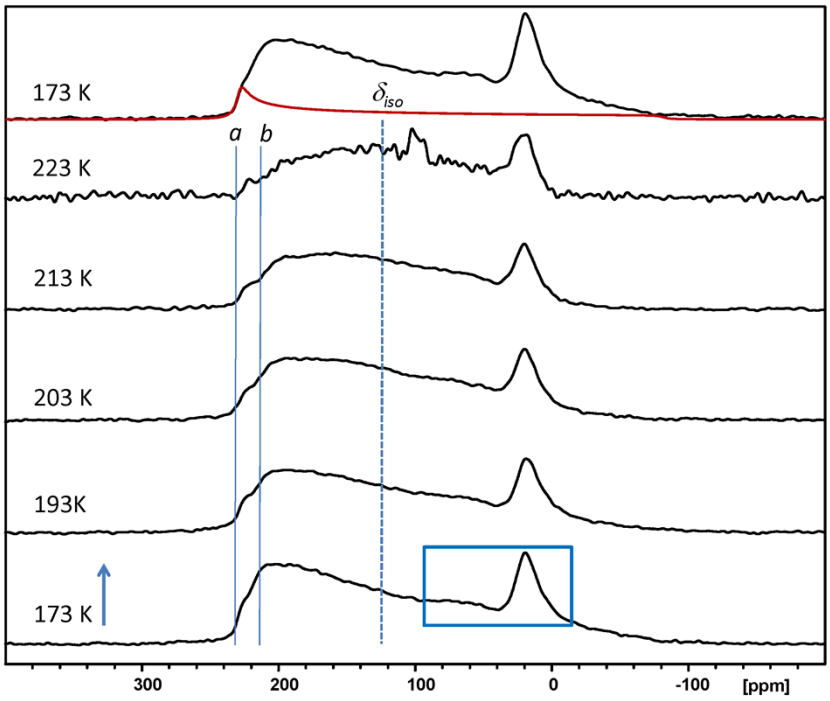

Figure S2. Variable temperature ^{13}C CP NMR spectra of $^{13}CO_2 \cdot TBAB \cdot 38H_2O$ hydrate obtained in stationary conditions at temperatures as indicated in a field of 4.7 T. Vertical arrow above the bottom spectrum indicates the direction of the temperature change. The observed changes in the spectra are completely reversible indicating preservation of CO_2. The vertical lines indicate the isotropic chemical shift for the CO_2 (δ_{iso}), and the positions of the perpendicular component $\delta_\perp$ of the CSA tensors (*a* and *b)*. Note that the position of singularity *a* changes very little with the temperature. Simulation shown under the top spectrum indicates the axially anisotropic signal corresponding to singularity *a* and the isotropic shift of 125 ppm. A box around portion of the bottom spectrum indicates the positions of signals from the TBAB.

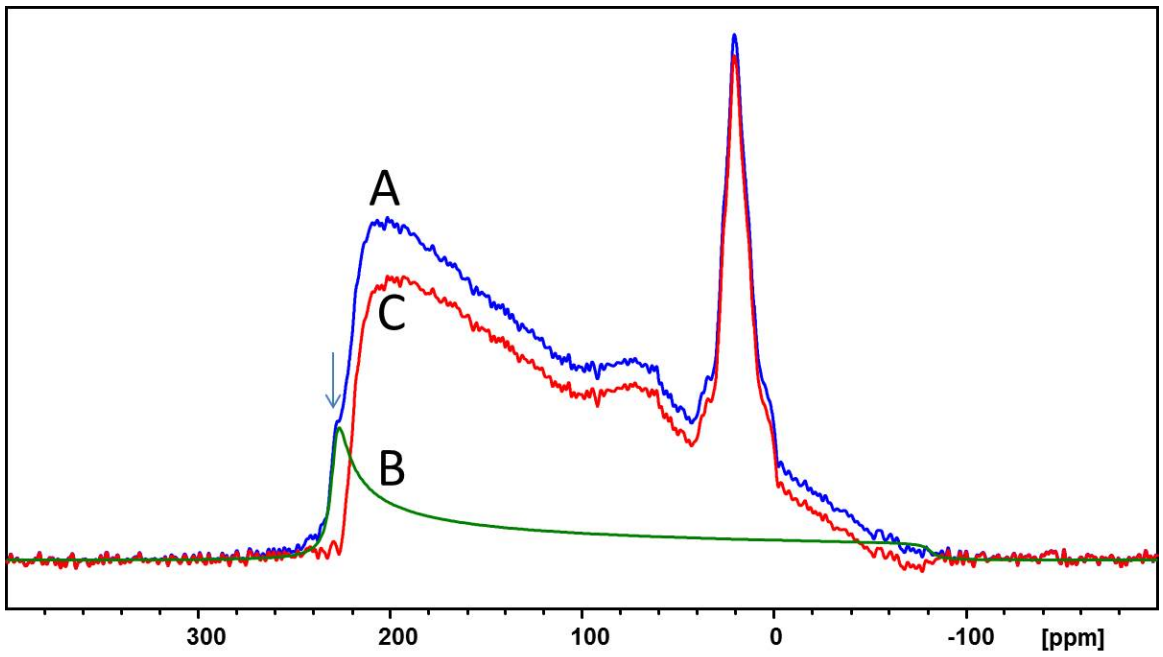

Figure S3. Spectrum A shows the stationary ^{13}C CP NMR spectra of $^{13}CO_2$-TBAB·$38H_2O$ hydrate obtained in a field of 9.4 T at 173 K. Simulation B shows axially anisotropic signal corresponding to singularity indicated by vertical arrow (perpendicular component $\delta_\perp$ of the CSA tensor) and the isotropic shift of 125 ppm from the MAS measurements. The positions of signals from the TBAB are as in Figure 2 of the manuscript. Trace C shows the difference between the experimental spectrum A and the simulation B.

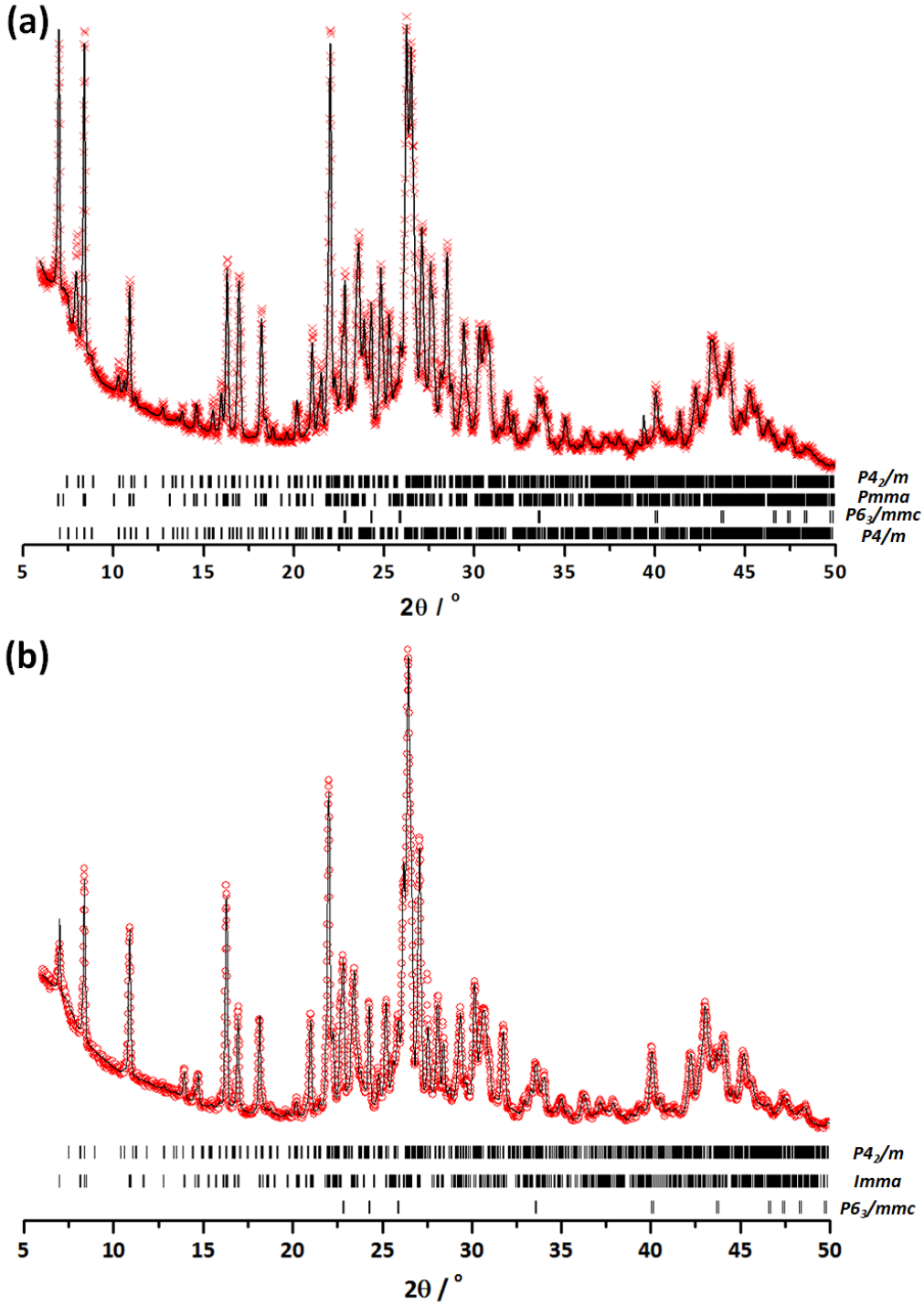

Figure S4. PXRD patterns and Le Bail fittings of 1 TBAB : 38 H_2O mixture recorded at 173 K (a) without CO_2 (χ^2 = 2.45, mixture of orthorhombic *Pmma* and tetragonal *P4/m* with small fraction of another tetragonal *P4₂/m*) and (b) with CO_2 (χ^2 = 2.89, mainly orthorhombic *Imma* with small fraction of tetragonal *P4₂/m*)

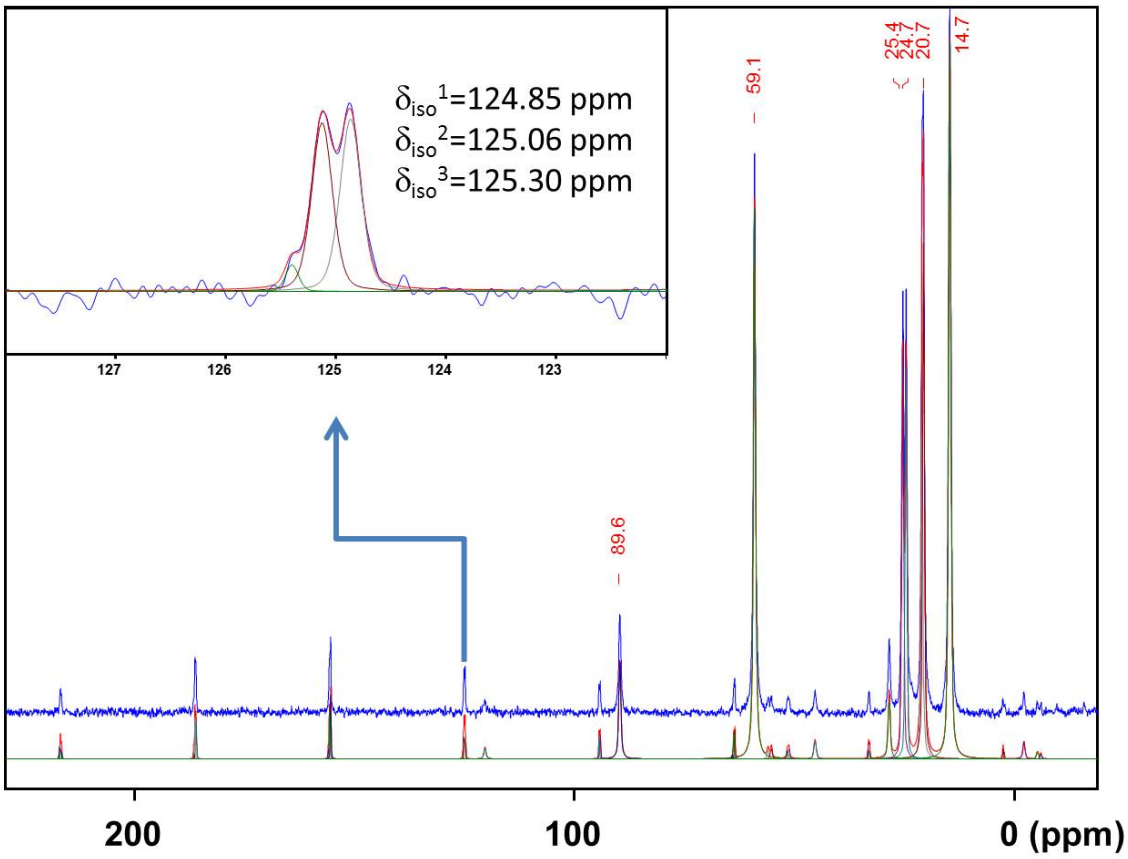

Figure S5. An experimental ^{13}C CP MAS spectrum of natural abundant $CO_2 \cdot TBAB \cdot 38H_2O$ hydrate obtained in a field of 9.4 T (Larmor frequency of 100.67 MHz) at 173 K. Spectrum B: Simulation of the experimental spectrum with a model accounting for spectral intensity spread in the spinning sidebands. The positions of the TBAB signals in the ^{13}C spectrum are at 59.1, 25.4 and 24.7, 20.7 and 14.7 ppm. The inset shows an expanded region for the isotropic signals of CO_2 in the hydrate cages.

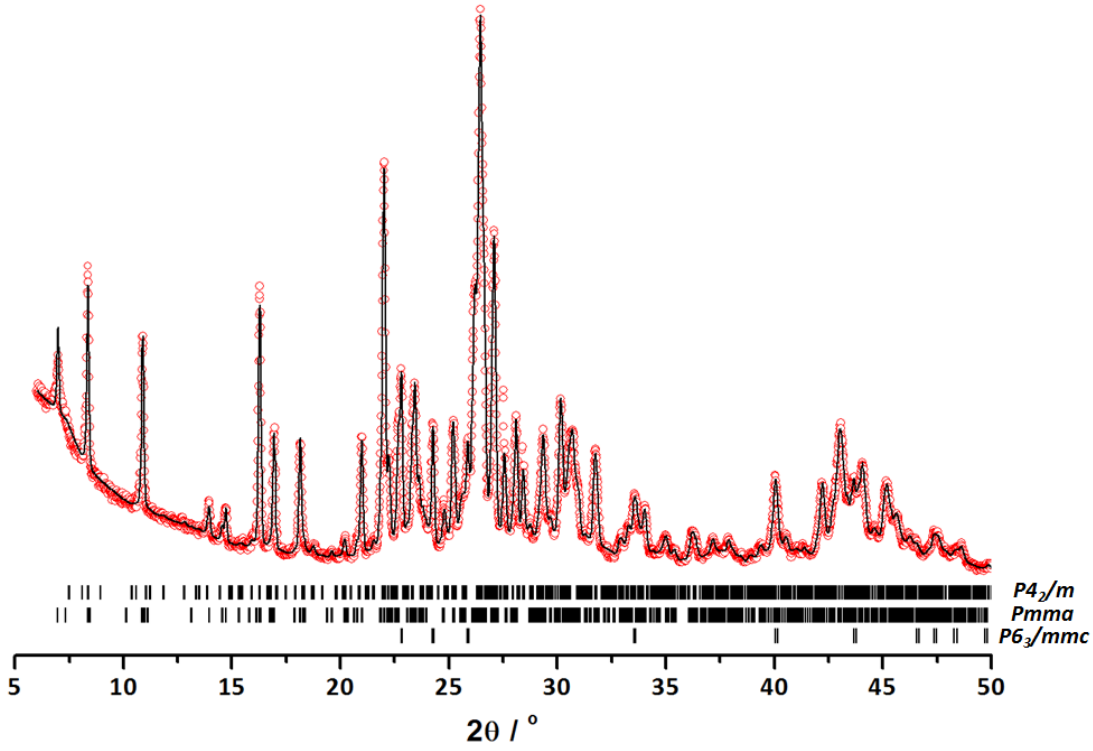

Figure S6. Le Bail fittings of the pattern shown in Figure S4 with *Pmma* indexing instead of *Imma* space group ($\chi^2 = 2.51$)

3. Computational Methods

Molecular dynamics simulations were performed using the single crystal X-ray structure of the TBAB ionic clathrate phase with incorporated CO_2 guests. The water proton positions in the ionic clathrate phase are disordered and were randomly chosen such that the ice rules were satisfied to the maximum extent possible and the unit cell dipole moment was minimized. Some tolerance for Bjerrum defects was built into the proton arrangement as water in ionic clathrates has greater freedom to rotate to more stable configurations during the MD run. The presence of the Br^- ions in lattice positions normally occupied by water can lead to the formation of Bjerrum defects in the lattice which facilitates water rotation. More detailed analysis of proton disorder in the ionic clathrate phases will remain for future work. In the crystal structure, the positions of the *n*-butyl chains of the *tetra*-butylammonium ion are disordered between two sets of sites with one set consistently chosen for each cation. The cation N atoms and anion Br^- are not disordered in the lattice. The initial CO_2 positions were chosen from one of the disordered positions in the dodecahedral cages of the crystal structure. There are two sets of dodecahedral (D, 5^{12}) cages in the unit cell (the D_A and D_B cages, see below) and their CO_2 occupancies and disorder are different. In the analysis of the geometric distribution and dynamics, these two groups of CO_2 molecules are considered separately. In the simulations, experimental occupancies of 53–87% for the D_A cages and 30–49% for the D_B cages are used. A second set of simulations with all D cages occupied are also performed. The specific D cage occupancies depend on the synthesis conditions of the ionic clathrate hydrate phase. A 2×2×4 replica of the unit cell was used in the simulations. There were a total of 2432 water, 64 TBAB, and 128 CO_2 molecules (with all D cages occupied) in the simulation. The details of the force fields used in the simulation are given in the Supporting Information. Constant volume–constant temperature NVT molecular dynamics simulations on periodic simulation cells were performed using the DL_POLY software program version 2.20.[25] The Nosé-Hoover thermostat[26] is used with a thermostat relaxation time of 0.2 ps. Long-range electrostatic interactions were calculated using the Ewald summation method[26] and all intermolecular interactions in the simulation box were calculated within a cut-off distance of R_{cutoff} = 13.0 Å. All simulations were performed with a time step of 1 fs for a total time

of 500 ps, with 10 ps of temperature scaled equilibration. Structural and dynamics parameters were extracted from the run times. Temperatures of 100 (X-ray structure determination temperature), 200, and 250 K with ambient pressure were used in the simulations.

The intermolecular van der Waals potentials between atoms *i* and *j* on different molecules are considered to be the sum of Lennard-Jones (LJ) and electrostatic point charges,

$$V(r_{ij}) = \sum_{i,j}\left\{4\varepsilon_{ij}\left[\left(\frac{\sigma_{ij}}{r_{ij}}\right)^{12} - \left(\frac{\sigma_{ij}}{r_{ij}}\right)^{6}\right] + \frac{q_i q_j}{4\pi\varepsilon_0 r_{ij}}\right\}, \qquad \text{(S1)}$$

where σ_{ij} and ε_{ij} are the distance and energy parameters of the *ij* pair separated by a distance of r_{ij} and q_i and q_j are the electrostatic point charges on the atoms. Water molecules of the clathrate were modeled using the TIP4P four-charge model,[27] while the tetrabutylammonium and bromine ions were modeled with the general AMBER force field,[28] and the force field for bromide by Canongia Lopes and Pádua.[29] The EMP2 potential[30] for carbon dioxide helper guest molecules. The values for the parameters σ_{ii} and ε_{ii} for selected atom types are given in Table S4. Potentials between unlike atoms are calculated using the standard combination rules, $\varepsilon_{ij} = (\varepsilon_{ii}\varepsilon_{jj})^{1/2}$ and $\sigma_{ij} = (\sigma_{ii} + \sigma_{jj})/2$. Partial electrostatic charges on the atoms of the guest molecules were determined from charges from electrostatic potential grid (CHELPG) calculations[31] with the Gaussian 09 suite of programs[32] at the B3LYP/6-311++G(*d*,*p*) level of theory. The complete set of guest point charges and Lennard-Jones parameters are given in Table S4.

The CO_2 guests were found to have restricted, but different spatial distribution / motion in D_A and D_B cages. The orientations of the CO_2 guest molecules in the D_A cages with respect to the lattice *b*-direction (as shown in Figure S7) and in the D_B cages with respect to the lattice *a*- and *c*-directions were sampled. The angle of the CO_2 molecular axis with respect to the foreshortened polar direction of the D_A cages is shown by θ which we sample to obtain orientation distribution of the CO_2 molecules, $p(\theta)$. The probability distribution $p(\theta)\cdot\sin\theta$ associated with this angle for CO_2 molecules in D_A cages at 100, 200, and 250 K are shown in Figure S7. The CO_2 molecules narrowly distributed with a spread of about 20° on each side of the 90° orientation. This constricted motion is also reflected by the relatively broad line

shape of the ^{13}C MAS solid-state NMR spectrum of the hydrate phase shown in Figure S2. The distributions become broader at higher temperatures which reflects the greater range of motion of the CO_2 molecules out of the equatorial plane of the D_A cages. This distribution should be compared to the D cages of the cubic structure I CO_2 clathrate hydrate where the CO_2 molecules are isotropically distributed as shown by the isotropic NMR lineshape of these guests.

Table S4. Atomic point charges and Lennard-Jones parameters for H_2O, CO_2, Br^-, and $N(C_4H_9)_4^+$. The AMBER labels are specified for the tetra-*n*-butylammonium atoms.

Atom / label	q / e	σ_{ii} / nm	ε_{ii} / kJ·mol^{-1}
O (H2O)	0.0	0.3153	0.6485
H (H2O)	+0.5200	0.000	0.000
M (H2O)	-1.0400	0.000	0.000
C (CO2)	+0.6512	0.2745	0.2489
O (CO2)	-0.3256	0.3017	0.7121
Br^-	-1.00	0.397	0.86
N(N4)	+0.570	0.325	0.711
C1 (C3)	-0.270	0.340	0.4577
H1 (HX)	+0.076	0.196	0.06568
C2 (C3)	+0.167	0.340	0.4577
H2 (HC)	-0.009	0.269	0.6571
C3 (C3)	+0.031	0.340	0.4577
H3 (HC)	+0.021	0.269	0.6571
C4 (C3)	-0.262	0.340	0.4577
H4 (HC)	+0.096	0.269	0.6571

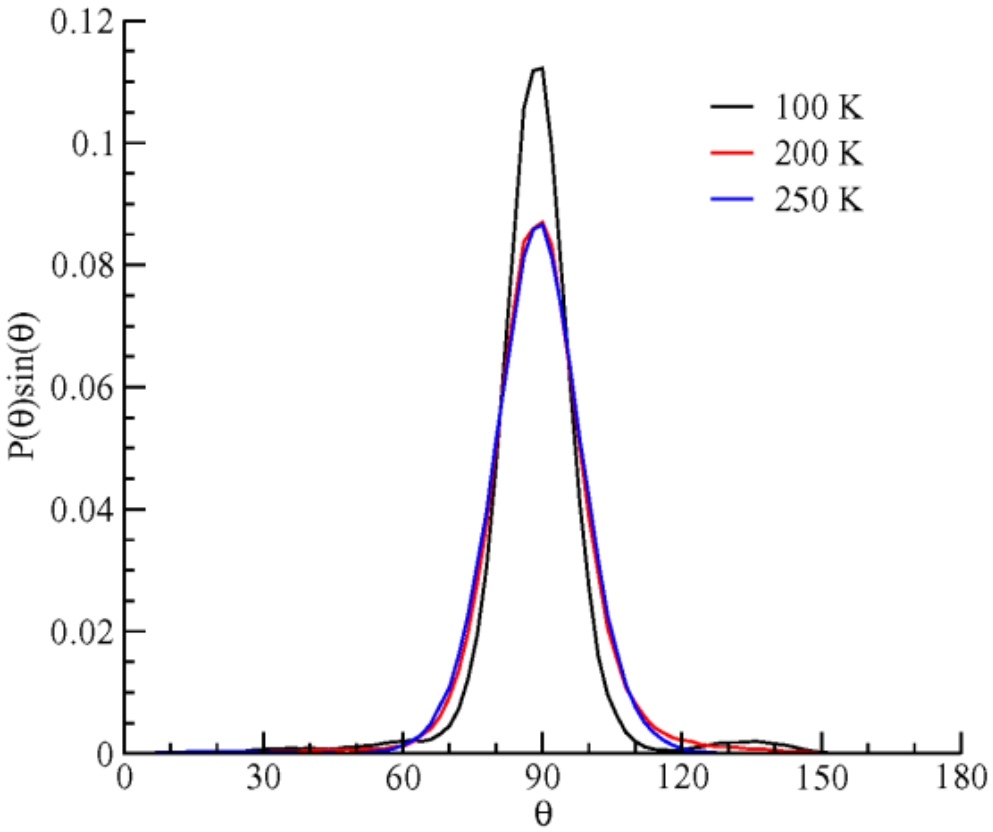

Figure S7. The narrow probability distribution functions for the polar angle θ of CO_2 molecules with the *b*-axis direction in the D_A cages.

References

[1] H. Oyama, W. Shimada, T. Ebinuma, T., Y. Kamata, S. Takeya, T. Uchida, J. Nagao, and H. Narita, *Fluid Phase Equilib*. **2005**, *234*, 131–135.

[2] K. Sato, H. Tokutomi, and R. Ohmura, Fluid Phase Equilib. **2013**, 337, 115-118.

[3] M. Arjmandi, A. Chapoy, and B. Tohidi, B. J. Chem. Eng. Data **2007**, 52, 2153–2158.

[4] S. Lee, S. Park, Y. Lee, J. Lee, H. Lee, and Y. Seo, Langmuir **2011**, 27, 10597–10603.

[5] N. Ye and P. Zhang, J. Chem. Eng. Data **2012**, 57, 1557–1562.

[6] S. Koyanagi and R. Ohmura, Cryst. Growth Des. **2013**, 13, 2087-2093.

[7] G. M. Sheldrick, Acta Crystallogr. **1990**, A46, 467.

[8] G. M. Sheldrick, Acta Crystallogr. **1993**, A49 (Suppl.), C53.

[9] G. Metz, X. L. Wu and S. O. Smith, *J. Magn. Reson., Ser. A* **1994**, *110*, 219–227.

[10] T. Bräuniger, P. Wormald and P. Hodgkinson, *Monatsh. Chem*. **2002**, *133*, 1549–1554.

[11] N. Sinha, C. V. Grant, C. H. Wu, A. A. De Angelis, S. C. Howell and S. J. Opella, *J. Magn. Reson.* **2005**, *177*, 197–202.

[12] D. Massiot, F. Fayon, M. Capron, I. King, S. Le Calvé, B. Alonso, J. O. Durand, B. Bujoli, Z. Gan and G. Hoatson, *Magn. Reson. Chem.* **2002**, *40*, 70–76.

[13] J. Rodriguez-Carvajal, *Physica B*, **1993**, *192*, 55–69.

[14] C. I. Ratcliffe and J. A. Ripmeester, *J. Phys. Chem.* **1986**, *90*, 1259-1263.

[15] K. A. Udachin, C. I. Ratcliffe and J. A. Ripmeester, *J. Phys. Chem. B*, **2001**, *105*, 4200-4204.

[16] S. Alavi, P. Dornan and T. K. Woo, *ChemPhysChem* **2008**, *9*, 911-919.

[17] J. A. Ripmeester and C. I. Ratcliffe, *Energ. Fuel.*, 1998, **12**, 197.;

[18] R. K. McMullan, G. A. Jeffrey and M. Bonamico, *J. Chem. Phys.* **1963**, *39*, 3295–3310.

[19] G. A. Jeffrey, in *Inclusion Compounds*, (Eds. J. L. Atwood, J. E. D. Davies and D. D. MacNicol), Academic Press: London, **1984**, Vol. 1, Chapter 5.

[20] L. A. Gaponenko, S. F. Solodovnikov, Y. A. Dyadin, L. S. Aladko and T. M. Polyanskaya, *Zh. Strukt. Khim.*, **1984**, *25*, 175-177.

[21] W. Shimada, M. Shiro, H. Kondo, S. Takeya, H. Oyama, T. Ebinuma and H. Narita, *Acta Crystall.* **2005**, *C61*, o65-066. We note that the structure reported for TBAB•38H2O in Ref. 20 is the same as that for tetra-isoamylammonium fluoride·38H2O (see Ref. 19). The older literature uses space group *Pbmm* rather than *Pmma*, so the *a*- and *b*-axes have been switched.

[22] W. Shimada, T. Ebinuma, H. Oyama, Y. Kamata and H. Narita, *J. Cryst. Growth* **2005**, *274*, 246–250.

[23] K. Shin, Y. Kim, T. A. Strobel, P. S. R. Prasad, T. Sugahara, H. Lee, E. D. Sloan, A. K. Sum and C. A. Koh, *J. Phys. Chem. A* **2009**, *113*, 6415–6418.

[24] K. A. Udachin, C. I. Ratcliffe, G. D. Enright and J. A. Ripmeester, *Angew. Chem. Int. Ed.* **2008**, *47*, 9704–9707.

[25] *DL_POLY 2.20*, T. R. Forester, W. Smith and I. T. Todorov, Eds.; CCLRC: Daresbury Laboratory, Daresbury, UK, **2008**.

[26] (a) D. Frenkel and B. Smit, *Understanding Molecular Simulation*, (Academic Press, San Diego, **2000**). (b) M. P. Allen and D. J. Tildesley, *Computer Simulation of Liquids*, (Oxford Science Publications, Oxford, **1987**).

[27] J. L. F. Abascal, E. Sanz, R. Garcia Fernandez, and C. Vega, *J. Chem. Phys.* **2005**, 122, 234511.

[28] W. D. Cornell, P. Cieplak, C. L. Bayly, I. R. Gould, K. M. Merz Jr., D. M. Ferguson, D. C. Spellmeyer, T. Fox, J. M. Caldwell, and P. A. Kollman, *J. Am. Chem. Soc.* **1995**, *117*, 5179–5197.

[29] J. N. Canongia Lopes and A. A. H. Pádua, *J. Phys. Chem. B* **2006**, *110*, 19586-19592.

[30] J. G. Harris and K. H. Yung, *J. Phys. Chem.* **1995**, *99*, 12021–12024.

[31] C. M. Breneman and K. B. Wiberg, *J. Comp. Chem.* **1990**, *11*, 361–373.

[32] Gaussian 09, Revision D.01, M. J. Frisch, G. W. Trucks, H. B. Schlegel, G. E. Scuseria, M. A. Robb, J. R. Cheeseman, G. Scalmani, V. Barone, B. Mennucci, G. A. Petersson, H. Nakatsuji, M. Caricato, X. Li, H. P. Hratchian, A. F. Izmaylov, J. Bloino, G. Zheng, J. L. Sonnenberg, M. Hada, M. Ehara, K. Toyota, R. Fukuda, J. Hasegawa, M. Ishida, T. Nakajima, Y. Honda, O. Kitao, H. Nakai, T. Vreven, J. A. Montgomery, Jr., J. E. Peralta, F. Ogliaro, M. Bearpark, J. J. Heyd, E. Brothers, K. N. Kudin, V. N.

Staroverov, R. Kobayashi, J. Normand, K. Raghavachari, A. Rendell, J. C. Burant, S. S. Iyengar, J. Tomasi, M. Cossi, N. Rega, J. M. Millam, M. Klene, J. E. Knox, J. B. Cross, V. Bakken, C. Adamo, J. Jaramillo, R. Gomperts, R. E. Stratmann, O. Yazyev, A. J. Austin, R. Cammi, C. Pomelli, J. W. Ochterski, R. L. Martin, K. Morokuma, V. G. Zakrzewski, G. A. Voth, P. Salvador, J. J. Dannenberg, S. Dapprich, A. D. Daniels, Ö. Farkas, J. B. Foresman, J. V. Ortiz, J. Cioslowski, and D. J. Fox, Gaussian, Inc., Wallingford CT, **2009**.